



This is the accepted manuscript made available via CHORUS. The article has been published as:

Direct evaluation of high neutron density environment using math

$\langle \sigma_{n,2n} \rangle$ reaction induced by
laser-driven neutron source

Takato Mori, Akifumi Yogo, Takehito Hayakawa, Seyed R. Mirfayzi, Zechen Lan, Yuki Abe, Yasunobu Arikawa, Daniil Golovin, Tianyun Wei, Yuki Honoki, Mitsuo Nakai, Kunioki Mima, Hiroaki Nishimura, Shinsuke Fujioka, and Ryosuke Kodama

Phys. Rev. C **104**, 015808 — Published 30 July 2021

DOI: [10.1103/PhysRevC.104.015808](https://doi.org/10.1103/PhysRevC.104.015808)

The Direct Evaluation of High Neutron Density Environment Using (n, 2n) Reaction Induced by Laser-driven Neutron Source

Takato Mori,¹ Akifumi Yogo,¹ Takehito Hayakawa,² Seyed R. Mirfayzi,^{1,3} Zechen Lan,¹ Yuki Abe,^{1,4} Yasunobu Arikawa,¹ Daniil Golovin,¹ Tianyun Wei,¹ Yuki Honoki,¹ Mitsuo Nakai,¹ Kunioki Mima,¹ Hiroaki Nishimura,^{1,5} Shinsuke Fujioka,¹ and Ryosuke Kodama¹

¹*Institute of Laser Engineering, Osaka University, Suita 565-0871, Japan*

²*National Institutes for Quantum and Radiological Science and Technology, Tokai 319-1106, Japan*

³*Blackett Laboratory, Imperial College London, London SW7 2AZ, UK.*

⁴*Graduate School of Engineering, Osaka University, Suita 565-0871, Japan and*

⁵*Fukui University of Technology, Fukui, 910-0028, Japan*

We demonstrate that (n, 2n) reactions are induced by a high-flux pulse of fast neutrons ($\sim 10^{10}$ neutrons in ~ 1 ns) provided from a Laser-driven Neutron Source (LDNS). The maximum energy of the broadband neutrons reaches a few tens MeV. Several kinds of metal targets are exposed to the fast neutrons. As a result, unstable isotopes such as ^{54}Mn , ^{58}Co , ^{175}Hf , and ^{196}Au are produced by (n, 2n) reactions and $^{180}\text{Hf}^m$, ^{181}Hf , ^{56}Mn , ^{198}Au , and ^{60}Co are produced by (n, γ) reactions. We evaluate the neutron fluence and energy spectrum using the activation method in conjunction with a time-of-flight (TOF) measurement. The neutron fluence is determined to be $(4.3 \pm 0.5) \times 10^8$ neutrons/cm² in the energy range from approximately 8 to 20 MeV at 8-mm downstream of the neutron source. The present scheme provides a method to evaluate high density neutrons seen in stellar environments, which are expected to be generated from future LDNSs.

I. INTRODUCTION

The development of the chirped pulse amplification [1] provided the technology of high power lasers realizing the intensity of 10^{23} Wcm⁻² [2][3], which can be used for ion acceleration based upon the interactions of high intense laser and plasma [4] [5] [6] [7] [8] [9] [10]. Nowadays, variable ion species such as proton, deuteron, and carbon are accelerated by the laser plasma interactions and their energies are reaching tens of MeV. Using laser-accelerated protons and deuterons, neutron pulses could be generated via nuclear reactions on a secondary target at its proximity such as the d(p, np)p and d(d, n)³He [11], ⁹Be(p, n)⁹B, ⁹Be(d, xn) [12] [13], ⁷Li(p, n)⁷Be, and (γ , n) reactions [14] [15]. Recently, neutron generation using d + Be reactions with deuterons accelerated from a deuterated plastic [(C₂D₂)_n, henceforth referred as CD] target with high intense laser were conducted [12] [13]. These neutron sources, termed by a laser-driven neutron sources (LDNSs), have remarkable features of brightness, short pulse width in order of sub-ns, and small size of a few cm³. The yield of neutrons reaches more than 10^{10} neutrons/sr in GSI [12] and the Los Alamos National Laboratory (LANL) [13]. These laser-accelerated ions and neutrons can be used for applications in wide fields of science and industry such as radiography [16][17], biology [18], and astrophysics [19][20]. Although maximum energies of neutrons generated by LDNSs reach a few tens MeV, it is possible to soften the neutron energies using a miniature moderator to make the energy spectrum suitable for different applications. Currently, epi-thermal neutrons (0.5 eV-100 keV) are demonstrated with a polystyrene moderator at the VULCAN laser facility [21], and thermal (around 25 meV) and cold neutrons (lower than 25 meV) were generated with a pure hydrogen moderator at the ILE [22]. At present, LDNSs have been expected as one of the next generation of short pulse neutron sources for various applications such as Neutron Resonance Absorption (NRA) [23], Boron Neutron Capture Therapy (BNCT) [24], and neutron imaging with Bragg edge transmission [25].

The laser-driven beams are also suitable for the study of stellar nucleosyntheses in astrophysics [26] [27]. Most elements heavier than iron are synthesized by major stellar nuclear reactions of slow neutron capture reactions (s process) [28], rapid neutron capture reaction (r process) [29], and successive photodisintegration reactions (γ process) [30]. To study the r process, Habs *et al.* have proposed to generate neutron-rich isotopes using nuclear fusion-fission reactions with heavy ions accelerated by interactions between high intense laser and heavy element materials such as ²³²Th [31]. Nuclear experiments using high intense neutrons generated by laser D+T nuclear fusion reactions at the National Ignition Facility (NIF) has been proposed to study the s process and the γ process [32]. The cross-sections of the ³He(d, p)⁴He reaction, which are important for understanding the Big-bang nucleosynthesis, was measured using the Texas Petawatt Laser [33]. In previous studies, the nuclear reaction cross sections have been measured mainly using beams provided from accelerators or nuclear reactors. While the conventional methods are

beneficial to obtain the nuclear reaction cross section, it lacks the ability to measure directly stellar nuclear reaction cross section, in particular, on the middle-heavy nuclei. This is because stellar nucleosyntheses proceed in high temperature environments such as $T \sim 10^{8-9}$ K [28,29,30] where nuclei are partly excited. However, in the previous conventional methods, nuclear reaction cross sections on the ground state of a nuclide of interest have been measured and stellar nuclear reaction cross sections on excited nuclei have been calculated theoretically. Hayakawa *et al.* [27] have proposed a method that nuclei in the primary target are excited in plasma generated by the first laser pulse and subsequently a laser-driven beam generated from the second target with another laser pulse is irradiated on the primary target to measure directly stellar nuclear reaction cross sections in hot plasma. In addition, although particles such as neutron or photon in stellar environments has a wide energy spread described by Planck or Fermi-Dirac distributions, it was presented that it is possible to generate a laser driven-beam having an energy spectrum similar to that in stellar environment [27]. These methods can be applied to the study of other nucleosynthesis processes such as the s and r processes. Furthermore, Hill and Wu have proposed a novel method that neutron-rich isotopes heavier than the initial isotopes by four neutrons are produced by successive neutron capture reactions with LDNSs [34]. These proposals and experimental demonstrations show that LDNSs have a large potential for the study of stellar nucleosyntheses, in particular, neutron capture reactions.

One of the key techniques for studying the nucleosynthesis is the measurement of the neutron energy spectrum. It can be performed via different methods such as the stacked CR-39 solid-state nuclear track detector [35] [36] and the neutron time-of-flight (TOF) with a scintillation detector [37]. The CR-39 detector is sensitive to neutrons in the energy region of 1-10 MeV. In the TOF method, it is possible to measure the energy spectrum of each laser shot and sensitive to more wide energy region. However, in both method the calibration to evaluate the absolute flux is required. We thus investigate a new method to evaluate the absolute neutron flux using a (n, 2n) reaction activation method in conjunction with the TOF measurement for LDNSs. The activation method has been known as a tool to measure precisely the number of unstable isotopes inside a target, used in nuclear physics and nuclear astrophysics [38] [39] [40] [41]. The activation method with (n, 2n) reactions is also useful for measurement of fast neutrons in an energy region of typically 10-20 MeV [42] [43] [44]. For example, the $^{197}\text{Au}(n, 2n)^{198}\text{Au}$ reaction is used to determine the ratio of down scattered neutrons relative to the primary neutron yield at the NIF [45] [46]. In the present work, we perform an activation experiment using (n, 2n) and (n, γ) reactions and a TOF measurement to evaluate neutron energy spectra for our LDNS. Metal targets of hafnium (Hf), manganese (Mn), gold (Au), cobalt (Co) are exposed to high energy neutrons generated from the LDNS. The γ -rays emitted following β -decay (or isomeric decay) of the unstable isotopes (or isomers) were measured. We evaluate the absolute neutron flux from the effective cross section obtained from the known cross sections and the neutron energy distribution obtained from the TOF measurement.

II. EXPERIMENTAL METHODS

The experiment was carried out using the petawatt laser for Fast Ignition Experiments (LFEX) laser system at the ILE, Osaka University. In LFEX experiments [47], four laser pulse with an intensity of 1×10^{19} W/cm² and 1.5×10^{19} W/cm² with a width of 1.5 ps in half width at half maximum (FWHM) were focused on a CD target with a thickness of 1.5 μm . On the laser focus spot, a strong quasi-static electric field up to 1 MV/ μm was generated on the rear side of the foil plasma [48], leading to ion acceleration. We used two shots (L3651 and L3658) for this study, the shot L3651 was used for the diagnostics of laser accelerated ions and the shot L3658 for the activation experiment with neutrons. The energy spectra of the protons and deuterons accelerated by the laser plasma interaction were measured by a Thomson parabola ion spectrometer [49] in the shot L3651. In the present LFEX experiment, protons and deuterons were accelerated up to 30 MeV/u and 10 MeV/u, respectively, with continuous energy distributions via the Boosted-Target Normal Sheath Acceleration (B-TNSA) mechanism [50]. After the energy measurements of the protons and deuterons, the experimental setup was changed to produce neutrons and measure neutron-induced reactions on activation targets. A ^9Be block (ϕ 5 mm \times 10mm) was placed at 2-mm distance behind the CD foil. The neutrons were produced primarily by (d, n) and (p, n) reactions on Be and the energies of the neutrons were in the range from sub-MeV to a few tens MeV. Figure 1 (a) shows a schematic view of the experimental layout. The activation targets were placed behind the Be neutron generator. As the activation targets, Hf ($\geq 97\%$) and Au (99.95%) discs (ϕ 9 mm \times 1mm) and Mn (99.999%, about 125 mm³) and Co (99.98%, about 125 mm³) shots were used. Figure 1 (b) shows the cross-sectional view of the activation targets. Au, Co and Mn are known as neutron flux monitor for both (n, γ) and (n, 2n) reactions. The Au target is suitable for neutron diagnostics because $^{197}\text{Au}(n, \gamma)^{198}\text{Au}$ could be used to record the number of thermal neutrons and the $^{197}\text{Au}(n, 2n)^{196}\text{Au}$ reaction could be used for the measurement of fast neutron flux. Measurements of the $^{55}\text{Mn}(n, \gamma)^{56}\text{Mn}$ reaction is suitable for LFEX experiments because the half-life of ^{56}Mn is 2.6 hour. Hf has many stable isotopes and isomers and has been used as a sample for the study of nuclear astrophysics [51] [52]. Table I shows the mass, size, and shape of the neutron-irradiated

targets and the natural isotopic abundances of the target nuclides.

To conduct TOF measurements of neutrons, a benzophenon-doped BBQ liquid scintillator (ϕ 60 mm \times 60 mm) with a Photomultiplier tube (Thron EMI 9902KBT) (PMT) [53] was placed at a position with a direction of 15 deg away from the laser axis and a 8.3-m distance from the target. The TOF detector was used to obtain the energy distribution of the neutrons. The wave signals from the PMT were recorded using an oscilloscope by shot by shot. The neutron energy spectrum for each laser shot was evaluated from each recorded wave using the procedure based upon the previous study [37]. After a cooling time of 15 minutes from the neutron generation laser shot L3658, the activated targets were moved to a position to measure γ -rays from the targets. The γ -rays were measured with high-purity germanium (HPGe) detectors. Natural background radiations were shielded by Pb blocks with a thickness of 10 cm and Cu plates with a thickness of 5 mm. We used three HPGe detectors, named Ge1, Ge2, and Ge3. The detection efficiencies of the HPGe detectors are approximately 30%, 50%, and 70% relative to a ϕ 3 inch \times 3 inch NaI(Tl) scintillation detector. The signals from these detectors were recorded with a multichannel analyzer (APG 7400A USB-MCA 4, TechnoAP). Typical dead time is lower than 0.02%. The energy resolutions and detection efficiencies of the HPGe detectors were calibrated using standard sources of ^{60}Co , ^{133}Ba , and ^{152}Eu . The energy resolutions of Ge1, Ge2, and Ge3 were 2.2, 2.5, and 2.4 keV in FWHM at 1.33 MeV, respectively.

III. EXPERIMENTAL RESULTS

We used the two laser shots of L3651 and L3658 for measuring of the energy spectra of laser accelerated ions and for the neutron induced reaction experiment, respectively. Figure 2 shows proton and deuteron signals recorded on an image plate (IP) placed behind the Thomson parabola ion spectrometer (a) and their energy spectra evaluated from the signals on the IP (b). The two ions are clearly separated as shown in Fig. 2(a). The proton and deuteron beam spectra exhibit the absolute number of these ions [49]. The energies of the deuterons are in the range from 2 MeV to 8 MeV, whereas the energies of the protons are in the range from 6 MeV to 30 MeV. Using the present Thomson parabola spectrometer, the detection lower limits for protons and deuterons are 2 MeV and 6 MeV, respectively. Because the threshold energy of the $^9\text{Be}(p, n)^9\text{B}$ reaction is 1.88 MeV, most protons could contribute to generation of neutrons. In the case of $d + ^9\text{Be}$ reactions, neutrons are predominantly generated by the $^9\text{Be}(d, n)^{10}\text{B}$ reaction and the break-up reactions. The average energy of the deuterons is lower than that of the protons and thus the deuterons more effectively contribute to generation of relatively low energy neutrons. Figure 3(a) shows the output signals from the scintillation detector. The signals of the neutrons are clearly separated from that of the prompt x-rays. We obtained the neutron energy spectrum from the scintillator output using the previously developed method [37]. In the previous study [37], the neutron fluence obtained from the TOF method was calibrated using bubble detectors. To obtain the neutron energy spectrum at the target position we corrected the transmission of the neutrons with the chamber wall with a thickness of 8 cm. Figure 3(b) shows the neutron energy spectrum obtained from the scintillator output in Fig. 3(a). The flux of the neutrons decreases with increasing neutron energy. In the TOF method, although the absolute value may not be well calibrated, it is considered that the energy distribution of neutrons is expected to be proportional to the voltage of the scintillator signal. This energy distribution was used to estimate effective (n, 2n) reaction cross sections on nuclides in the activation targets.

Figure 4 shows the spectra of the γ -ray radiated from the activated targets, which were measured by the HPGe detectors. These spectra show that the radioactive isotopes and the isomer of $^{175,181}\text{Hf}$, $^{196,198}\text{Au}$, $^{54,56}\text{Mn}$, $^{58,60}\text{Co}$ and $^{180}\text{Hf}^m$ were generated by laser-driven neutron irradiation. The unstable isotopes of ^{181}Hf , ^{198}Au , ^{56}Mn , and ^{60}Co and the isomer of $^{180}\text{Hf}^m$ were produced by neutron capture reactions, whereas ^{175}Hf , ^{196}Au , ^{58}Co , and ^{54}Mn were synthesized by (n, 2n) reactions with fast neutrons. ^{175}Hf may be also produced by the neutron capture reaction on a stable isotope ^{174}Hf but ^{175}Hf is expected to be produced predominantly by the (n, 2n) reaction on a stable isotope ^{176}Hf because the isotopic abundance of ^{176}Hf is 5.26% higher than the ^{174}Hf abundance of 0.16% by a factor of 32. Table II shows the energies of the measured γ -rays and their emission probability per decay. For some unstable isotopes (isomers) such as ^{196}Au and $^{180}\text{Hf}^m$, several γ -rays are radiated. In such cases, the weighted average of the measured γ -rays was adopted for the estimation of its reaction rate. As shown in Fig. 4, there are many γ -rays emitted from natural background radiation sources [54]. We summarized them in Table III. For $^{180}\text{Hf}^m$, $^{196,198}\text{Au}$, and ^{56}Mn , the γ -rays of each nuclide were measured for about twice time of the half-life of the nuclide, whereas for $^{175,181}\text{Hf}$, ^{54}Mn , and $^{58,60}\text{Co}$ with half-lives longer than 70 d, the γ -ray measurements were performed for about three months. Figure 5 (a) and (b) shows the decay curves of the 333-keV and 355-keV γ -rays from ^{196}Au and the 412-keV γ -ray from ^{198}Au , respectively. These decay curves are consistent with their half-lives within their uncertainties. The peak areas of γ -rays were counted for the evaluation of the numbers of the generated unstable nuclei and the nuclear reaction rate per nucleus. Figure 6 shows the efficiency curves of the HPGe detectors. Table IV shows the nuclear reaction rate per nucleus, which corresponds to the unstable isotope (or isomer) production rate per nucleus. The number of the neutrons produced by the laser shot can be obtained by dividing the nuclear reaction rate on a nuclide

by the effective (n, 2n) reaction cross section of the nuclide.

IV. DISCUSSION

The focus of our research was to develop an evaluation method of the flux of fast neutrons with energies more than approximately 8 MeV provided from LDNSs. We investigated the use of the activation method with (n, 2n) reactions because the activation method has been known as one of the methods to evaluate precisely the number of radioactive nuclides of interest. Using LDNSs, it is possible to place activation targets close to a neutron source with a distance of a few cm and thus a large number of neutrons could be incident on the targets. The decay rate of an unstable isotope (or isomer) of interest, which is correlated with the isotope (isomer) generation rate per target nucleus, was measured by the HPGe detectors after the neutron generation shot L3658. The isotope generation rate per target nucleus r can be calculated from the peak area of a γ -ray radiated from an unstable isotope A using the following relation:

$$r = \frac{A}{\varepsilon I_{\gamma}} \frac{M}{N_A \theta m} (e^{-\lambda t_1} - e^{-\lambda t_2})^{-1}, \quad (1)$$

where ε is the detection efficiency including the geometric factor related to the sample position, I_{γ} is the γ -ray emission probability, M is the atomic mass of the target isotope, N_A is the Avogadro number, θ is the isotopic abundance of the target isotope, m is the weight of the sample, λ is the decay constant in unit of s^{-1} , t_1 is the measurement started time, and t_2 is the measurement finished time.

To evaluate the (n, 2n) reaction cross section, we used the neutron energy distribution measured by the TOF method on the shot L3658. It was reported that the neutron spectrum $\phi(E)$ provided from LDNSs could be reproduced using the two-temperature distribution as

$$\phi(E) = AE^{0.5} e^{-E/T_1} + BE^{0.5} e^{-E/T_2}, \quad (2)$$

where A and B are the coefficients for normalization, E is the neutron energy, T_1 and T_2 are the neutron average temperatures. We obtained the two temperature of $T_1=0.39$ MeV and $T_2=2.54$ MeV. We should note that we used the measured neutron energy distribution obtained directly from the scintillator output in Fig. 3(b) in the following analysis. In the activation method with an incident beam with wide spread energy, the number of the incident particles can be evaluated using the total number of unstable isotopes generated by a nuclear reaction and its effective nuclear reaction cross section. The effective (n, 2n) reaction cross section on a nuclide of interest was used for the estimation of the total number of the (n, 2n) reactions on the target. The effective (n, 2n) reaction cross section S was calculated with following relation:

$$S = \sum_{i=0}^k \Phi(E_i) \times \sigma(E_i), \quad (3)$$

where $\Phi(E_i)$ is the dn in an energy region from E_i to $E_i+\Delta E$ obtained from the neutron energy spectrum measured by the TOF method, which is not the same as $\phi(E)$ corresponding to dn/dE , $\sigma(E_i)$ is the (n, 2n) reaction cross section at the neutron energy E_i , of which the energy width corresponds to the energy bin used in the JENDL-4.0 [48], E_0 is the threshold energy of the (n, 2n) reaction, and E_k is 20 MeV which is the upper limit energy of the nuclear database. Using Eq. (3), we obtain the effective (n, 2n) cross sections from the neutron energy distribution in the energy range from E_0 to 20 MeV and the (n, 2n) reaction cross section $\sigma(E_i)$. Figure 7 shows the (n, 2n) reaction cross sections on ^{176}Hf , ^{197}Au , ^{55}Mn , and ^{59}Co taken from the JENDL 4.0 nuclear data library [55], the measured neutron energy spectrum, and their products corresponding to the effective reaction rates. The fast neutron fluence n can be given by $n = (r/S)/D$ in unit of neutrons/cm², where D is the coefficient for the correction for scattering inside the target. The coefficient D was estimated by the PHITS simulation code [56]. According to the Eq. (3), the error of $\Phi(E_i)$ directly affects to the error of S . In the present study, we only take the errors originating from $\Phi(E_i)$ but the errors of the cross sections taken from the JENDL-4.0 was not in the calculation because it is expected that the shifts of the cross sections at different energies are canceled out. Using the total error of $\Phi(E_i)$, the relative error of S were estimated $\pm 1.9\%$, $\pm 0.7\%$, $\pm 1.5\%$, and $\pm 1.2\%$ for the $^{55}\text{Mn}(n, 2n)^{54}\text{Mn}$, $^{59}\text{Co}(n, 2n)^{58}\text{Co}$, $^{176}\text{Hf}(n, 2n)^{175}\text{Hf}$, and $^{197}\text{Au}(n, 2n)^{196}\text{Au}$ reactions, respectively. Note that the statistic errors of the peak areas of the γ -rays of ^{196}Au were smaller than those of ^{175}Hf , ^{54}Mn , and ^{58}Co .

From the results of the activation method, we obtained the neutron fluence n in unit of neutrons/cm². The decreases of the solid angle of the target from the neutron generation point and the measured neutron fluences are in

good agreement as shown in Fig. 8(a). To compare the neutron yield for different nuclides we convert the unit from neutron fluence n neutrons/cm² to neutron yield n_{sr} neutrons/sr using the following formula:

$$n_{sr} = \frac{n}{\Omega}, \quad (4)$$

where Ω is the coefficient for the correction of the solid angle of the target. Table V shows the neutron fluence obtained by the (n, 2n) activation method and the parameters for the calculations. The neutron yields evaluated from different targets are in good agreement within their uncertainties as shown in Fig. 8(b). The average neutron yield was obtained from the neutron yields of the four targets. The neutron yields obtained by the activation method was corrected with the geometric factors. The neutron yield obtained from the present activation method is $(5.4 \pm 0.5) \times 10^8$ neutrons/sr in the energy range of approximately 8 to 20 MeV, whereas that evaluated only from the TOF method is $(6.1 \pm 1.2) \times 10^8$ neutrons/sr. These yields are in good agreement with each other within their uncertainties. This result reveals that the TOF method is reliable on evaluating the absolute fluence of neutrons in the energy range of approximately 8-20 MeV.

We measured γ -rays from the unstable isotopes produce by the (n, γ) reactions. As mentioned previously, we were not able to measure the neutron energy spectrum lower than 1 MeV in the present experiment. Thus, it is difficult to evaluate the low-energy neutron flux using the presently developed method. To estimate the neutron flux, we first assume that all the unstable isotopes were produced by (n, γ) reactions with thermal neutrons, but the obtained neutron fluxes are inconsistent. They are $(6.6 \pm 0.9) \times 10^6$ neutrons/sr, $(1.65 \pm 0.25) \times 10^7$ neutrons/sr, $(9.4 \pm 1.1) \times 10^5$ neutrons/sr, and $(6.6 \pm 1.3) \times 10^7$ neutrons/sr for ¹⁹⁸Au, ¹⁸¹Hf, ⁵⁶Mn, and ⁶⁰Co, respectively. This can be explained by the fact that we did not use a moderator to soften neutron energies. Next, with the assumption that these nuclides were generated by 1-MeV energy neutrons, we obtained the fluxes of $(8.4 \pm 1.2) \times 10^8$ neutrons/sr, $(5.3 \pm 0.8) \times 10^8$ neutrons/sr, $(5.5 \pm 0.7) \times 10^8$ neutrons/sr, and $(2.1 \pm 0.4) \times 10^{10}$ neutrons/sr for ¹⁹⁸Au, ¹⁸¹Hf, ⁵⁶Mn, and ⁶⁰Co, respectively. In this case, the fluxes except that of ⁶⁰Co have relatively similar values. These results suggest that these nuclides were probably produced by high energy neutrons up to a few MeV rather than thermal neutrons. To evaluate neutron fluxes using (n, γ) reactions, we should decrease the detection lower limit in the TOF detector.

Although we measured the (n, 2n) reactions in the present study, it is possible to measure the fluences of neutrons higher than 20 MeV with the activation method using (n, 3n) and (n, 4n) nuclear reactions. Furthermore, when the energy spectrum of neutrons provided from LDNSs is more precisely measured with the TOF method, the activation method can be used for measuring the integrated neutron capture cross sections in the energy range of MeV. As presented previously, novel laser experiments to study nucleosynthesis under high-dense neutron environments such as the r-process have been proposed [27][31][33][34] and it is expected to perform them in future. One of the key parameters for these studies is the measurement of the neutron energy spectrum. The present method of the activation method in conjunction with the TOF spectrum contributes to them.

V. SUMMARY

We evaluated the yield of neutrons from laser driven neutron sources (LDNS) at the ILE in Osaka University using the activation method in conjunction with the time-of-flight (TOF) method. We measured decay γ -rays following β -decay (isomeric decay) of the unstable isotopes generated with the ⁵⁵Mn(n, 2n)⁵⁴Mn, ⁵⁹Co(n, 2n)⁵⁸Co, ¹⁷⁶Hf(n, 2n)¹⁷⁵Hf, and ¹⁹⁷Au(n, 2n)¹⁹⁶Au reactions. Nuclear reaction rate per nucleus for each nuclide was estimated from the γ -ray intensities and the neutron energy distribution obtained from the TOF method. We obtained the neutron flux of $(5.4 \pm 0.5) \times 10^8$ neutrons/sr in the energy range of approximately 8 to 20 MeV. We also obtained that of $(6.1 \pm 1.2) \times 10^8$ neutrons/sr only from the TOF method. The result from the activation method is in good agreement with the TOF measurement. This result reveals that the activation method using (n, 2n) reactions in conjunction with the TOF method is a useful tool to estimate fast neutron flux and energy spectrum. Furthermore, the present method can measure integral nuclear reaction cross sections in MeV energy region.

ACKNOWLEDGMENTS

The authors gratefully acknowledge the support of the LFEX development and operation group, the target fabrication group, and the plasma diagnostics operation group of the Institute of Laser Engineering, Osaka University. This work was funded by A-STEP (AS2721002c) commissioned by JST.

REFERENCES

- [1] D. Strickland and G. Mourou, *Compression of Amplified Chirped Optical Pulses*, Opt. Commun. **56**, 219 (1985).
- [2] G. A. Mourou, T. Tajima, and S. V. Bulanov, *Optics in the Relativistic Regime*, Rev. Mod. Phys. **78**, 309 (2006).
- [3] K. A. Tanaka, K. M. Spohr, D. L. Balabanski, S. Balascuta, L. Capponi, M. O. Cernaianu, M. Cuciuc, A. Cucoanes, I. Dancus, A. Dhal *et al.*, *Current Status and Highlights of the ELI-NP Research Program*, Matter Radiat. Extrem. **5**, 024402 (2020).
- [4] S. P. Hatchett, C. G. Brown, T. E. Cowan, E. A. Henry, J. S. Johnson, M. H. Key, J. A. Koch, A. B. Langdon, B. F. Lasinski, R. W. Lee *et al.*, *Electron, Photon, and Ion Beams from the Relativistic Interaction of Petawatt Laser Pulses with Solid Targets*, Phys. Plasmas **7**, 2076 (2000).
- [5] R. A. Snavely, M. H. Key, S. P. Hatchett, I. E. Cowan, M. Roth, T. W. Phillips, M. A. Stoyer, E. A. Henry, T. C. Sangster, M. S. Singh *et al.*, *Intense High-Energy Proton Beams from Petawatt-Laser Irradiation of Solids*, Phys. Rev. Lett. **85**, 2945 (2000).
- [6] S. C. Wilks, A. B. Langdon, T. E. Cowan, M. Roth, M. Singh, S. Hatchett, M. H. Key, D. Pennington, A. MacKinnon, and R. A. Snavely, *Energetic Proton Generation in Ultra-Intense Laser-Solid Interactions*, Phys. Plasmas **8**, 542 (2001).
- [7] T. Esirkepov, M. Borghesi, S. V. Bulanov, G. Mourou, and T. Tajima, *Highly Efficient Relativistic-Ion Generation in the Laser-Piston Regime*, Phys. Rev. Lett. **92**, 175003 (2004).
- [8] A. Henig, S. Steinke, M. Schnürer, T. Sokollik, R. Hörlein, D. Kiefer, D. Jung, J. Schreiber, B. M. Hegelich, X. Q. Yan *et al.*, *Radiation-Pressure Acceleration of Ion Beams Driven by Circularly Polarized Laser Pulses*, Phys. Rev. Lett. **103**, 245003 (2009).
- [9] S. Steinke, A. Henig, M. Schnürer, T. Sokollik, P. V. Nickles, D. Jung, D. Kiefer, R. Hörlein, J. Schreiber, T. Tajima *et al.*, *Efficient Ion Acceleration by Collective Laser-Driven Electron Dynamics with Ultra-Thin Foil Targets*, Laser Part. Beams **28**, 215 (2010).
- [10] W. P. Wang, B. F. Shen, X. M. Zhang, X. F. Wang, J. C. Xu, X. Y. Zhao, Y. H. Yu, L. Q. Yi, Y. Shi, L. G. Zhang *et al.*, *Cascaded Target Normal Sheath Acceleration*, Phys. Plasmas **20**, 113107 (2013).
- [11] S. Kar, A. Green, H. Ahmed, A. Alejo, A. P. L. Robinson, M. Cerchez, R. Clarke, D. Doria, S. Dorkings, J. Fernandez *et al.*, *Beamed Neutron Emission Driven by Laser Accelerated Light Ions*, New J. Phys. **18**, 053002 (2016).
- [12] A. Kleinschmidt, V. Bagnoud, O. Deppert, A. Favalli, S. Frydrych, J. Hornung, D. Jahn, G. Schaumann, A. Tebartz, F. Wagner *et al.*, *Intense, Directed Neutron Beams from a Laser-Driven Neutron Source at PHELIX*, Phys. Plasmas **25**, 053101 (2018).
- [13] A. Favalli, N. Guler, D. Henzlova, S. Croft, K. Falk, D. C. Gautier, K. D. Ianakiev, M. Iliev, S. Palaniyappan, M. Roth *et al.*, *Characterizing Laser-Plasma Ion Accelerators Driving an Intense Neutron Beam via Nuclear Signatures*, Sci. Rep. **9**, 2004 (2019).
- [14] D. Habs, T. Tajima, J. Schreiber, C. P. J. Barty, M. Fujiwara, and P. G. Thirolf, *Vision of Nuclear Physics with Photo-Nuclear Reactions by Laser-Driven γ Beams*, Eur. Phys. J. D **55**, 279 (2009).
- [15] Y. Arikawa, M. Utsugi, M. Alessio, T. Nagai, Y. Abe, S. Kojima, S. Sakata, H. Inoue, S. Fujioka, Z. Zhang *et al.*, *High-Intensity Neutron Generation via Laser-Driven Photonuclear Reaction*, Plasma Fusion Res. **10**, 2404003 (2015).
- [16] L. Romagnani, J. Fuchs, M. Borghesi, P. Antici, P. Audebert, F. Ceccherini, T. Cowan, T. Grismayer, S. Kar, A. Macchi *et al.*, *Dynamics of Electric Fields Driving the Laser Acceleration of Multi-MeV Protons*, Phys. Rev. Lett. **95**, 195001 (2005).
- [17] M. Borghesi, D. H. Campbell, A. Schiavi, M. G. Haines, O. Willi, A. J. MacKinnon, P. Patel, L. A. Gizzi, M. Galimberti, R. J. Clarke *et al.*, *Electric Field Detection in Laser-Plasma Interaction Experiments via the Proton Imaging Technique*, Physics of Plasmas **9**, 2214 (2002).
- [18] A. Yogo, K. Sato, M. Nishikino, M. Mori, T. Teshima, H. Numasaki, M. Murakami, Y. Demizu, S. Akagi, S. Nagayama *et al.*, *Application of Laser-Accelerated Protons to the Demonstration of DNA Double-Strand Breaks in Human Cancer Cells*, Appl. Phys. Lett. **94**, 181502 (2009).
- [19] H. Chen, S. C. Wilks, D. D. Meyerhofer, J. Bonlie, C. D. Chen, S. N. Chen, C. Courtois, L. Elbertson, G. Gregori, W. Kruer *et al.*, *Relativistic Quasimonoenergetic Positron Jets from Intense Laser-Solid Interactions*, Phys. Rev. Lett. **105**, 015003 (2010).

- [20] Y. J. Gu, F. Pegoraro, P. V. Sasorov, D. Golovin, A. Yogo, G. Korn, and S. V. Bulanov, *Electromagnetic Burst Generation during Annihilation of Magnetic Field in Relativistic Laser-Plasma Interaction*, Sci. Rep. **9**, 19462 (2019).
- [21] S. R. Mirfayzi, A. Alejo, H. Ahmed, D. Raspino, S. Ansell, L. A. Wilson, C. Armstrong, N. M. H. Butler, R. J. Clarke, A. Higginson *et al.*, *Experimental Demonstration of a Compact Epithermal Neutron Source Based on a High Power Laser*, Appl. Phys. Lett. **111**, 044101 (2017).
- [22] S. R. Mirfayzi, A. Yogo, Z. Lan, T. Ishimoto, A. Iwamoto, M. Nagata, M. Nakai, Y. Arikawa, Y. Abe, D. Golovin *et al.*, *Proof-of-Principle Experiment for Laser-Driven Cold Neutron Source*, Sci. Rep. **10**, 20157 (2020).
- [23] D. P. Higginson, J. M. McNaney, D. C. Swift, T. Bartal, D. S. Hey, R. Kodama, S. Le Pape, A. MacKinnon, D. Mariscal, H. Nakamura *et al.*, *Laser Generated Neutron Source for Neutron Resonance Spectroscopy*, Phys. Plasmas **17**, 100701 (2010).
- [24] M. F. Hawthorne, *New Horizons for Therapy Based on the Boron Neutron Capture Reaction*, Mol. Med. Today **4**, 174 (1998).
- [25] Y. Kiyanagi, *Neutron Imaging at Compact Accelerator-Driven Neutron Sources in Japan*, J. Imaging **4**, 55 (2018).
- [26] S. V. Bulanov, T. Z. Esirkepov, D. Habs, F. Pegoraro, and T. Tajima, *Relativistic Laser-Matter Interaction and Relativistic Laboratory Astrophysics*, Eur. Phys. J. D **55**, 483 (2009).
- [27] T. Hayakawa, T. Nakamura, H. Kotaki, M. Kando, T. Kajino, *Explosive Nucleosynthesis Study Using Laser Driven γ -ray Pulses*, Quantum Beam Sci. **1**, 3 (2017).
- [28] F. Käppeler, R. Gallino, S. Bisterzo, and W. Aoki, *The s Process: Nuclear Physics, Stellar Models, and Observations*, Rev. Mod. Phys. **83**, 157 (2011).
- [29] Y. Z. Qian and G. J. Wasserburg, *Where, Oh Where Has the r-process Gone?*, Phys. Rep. **442**, 237 (2007).
- [30] T. Hayakawa, N. Iwamoto, T. Shizuma, T. Kajino, H. Umeda, and K. Nomoto, *Evidence for Nucleosynthesis in the Supernova γ Process: Universal Scaling for p Nuclei*, Phys. Rev. Lett. **93**, 16 (2004).
- [31] D. Habs, P. G. Thirolf, M. Gross, K. Allinger, J. Bin, A. Henig, D. Kiefer, W. Ma, and J. Schreiber, *Introducing the Fission-Fusion Reaction Process: Using a Laser-Accelerated Th Beam to Produce Neutron-Rich Nuclei towards the N=126 Waiting Point of the r-Process*, Appl. Phys. B Lasers Opt. **103**, 471 (2011).
- [32] L. A. Bernstein, D. L. Bleuel, J. A. Caggiano, C. Cerjan, R. J. Fortner, J. Gostic, P. M. Grant, N. Gharibyan, C. Hagmann, R. Hatarik *et al.*, *Low Energy Neutron Measurements in High Energy Density Plasmas Using the National Ignition Facility*, Plasma Fusion Res. **9**, 4404101 (2014).
- [33] M. Barbui, W. Bang, A. Bonasera, K. Hagel, K. Schmidt, J. B. Natowitz, R. Burch, G. Giuliani, M. Barbarino, H. Zheng *et al.*, *Measurement of the Plasma Astrophysical S Factor for the ${}^3\text{He}(d,p){}^4\text{He}$ Reaction in Exploding Molecular Clusters*, Phys. Rev. Lett. **111**, 082502 (2013).
- [34] P. Hill and Y. Wu, *Exploring Laser-Driven Neutron Sources for Neutron Capture Cascades and the Production of Neutron-Rich Isotopes*, Phys. Rev. C **103**, 014602 (2021).
- [35] K. Oda, M. Ito, H. Miyake, M. Michijima, and J. Yamamoto, *Track Formation in CR-39 Detector Exposed to D-T Neutrons*, Nuclear Instruments and Methods in Physics Research **B35**, 50 (1988).
- [36] S. Cavallaro, *Fast Neutron Efficiency in CR-39 Nuclear Track Detectors*, Rev. Sci. Instrum. **86**, 036103 (2015).
- [37] S. R. Mirfayzi, S. Kar, H. Ahmed, A. G. Krygier, A. Green, A. Alejo, R. Clarke, R. R. Freeman, J. Fuchs, D. Jung *et al.*, *Calibration of Time of Flight Detectors Using Laser-Driven Neutron Source*, Rev. Sci. Instrum. **86**, 073308 (2015).
- [38] A. Shor, M. Tessler, A. Plompen, A. Arenshtam, O. Aviv, D. Berkovits, M. Brandis, Y. Eisen, I. Eliyahu, G. Feinberg *et al.*, *Bismuth Activation with Quasi-Maxwellian Neutrons at $kT \sim 30$ keV*, Phys. Rev. C **96**, 055805 (2017).
- [39] T. Heftrich, M. Weigand, C. E. Düllmann, K. Eberhardt, S. Fiebiger, J. Glorius, K. Göbel, C. Guerrero, R. Haas, S. Heinitz *et al.*, *Thermal (n,γ) Cross Section and Resonance Integral of ${}^{171}\text{Tm}$* , Phys. Rev. C **99**, 065810 (2019).
- [40] C. Guerrero, J. Leredegui-Marco, M. Paul, M. Tessler, S. Heinitz, C. Domingo-Pardo, S. Cristallo, R. Dressler, S. Halfon, N. Kivel, U. Köster *et al.*, *Neutron Capture on the S-Process Branching Point ${}^{171}\text{Tm}$ via Time-of-Flight and Activation*, Phys. Rev. Lett. **125**, 142701 (2020).

- [41] K. Göbel, C. Beinrucker, B. Brückner, P. Erbacher, S. Fiebiger, M. Fonseca, M. Heftrich, T. Heftrich, F. Käppeler, A. Krása *et al.*, *Neutron Activation of ^{69}Ga and ^{71}Ga at $k_B T \approx 25 \text{ keV}$* , Phys. Rev. C **103**, 025802 (2021).
- [42] J. Soter, M. Bhike, S. W. Finch, Krishichayan, and W. Tornow, *Measurements of the $^{169}\text{Tm}(n,2n)^{168}\text{Tm}$ Cross Section from Threshold to 15 MeV*, Phys. Rev. C **96**, 064619 (2017).
- [43] A. Gandhi, A. Sharma, A. Kumar, R. Pachua, B. Lalremruata, S. V. Suryanarayana, L. S. Danu, T. Patel, S. Bishnoi, and B. K. Nayak, *Measurement of (n,γ) , (n,p) , and $(n,2n)$ Reaction Cross Sections for Sodium, Potassium, Copper, and Iodine at Neutron Energy $14.92 \pm 0.02 \text{ MeV}$ with Covariance Analysis*, Phys. Rev. C **102**, 014603 (2020).
- [44] E. Georgali, N. Patronis, A. Anastasiadis, X. Aslanoglou, M. Axiotis, Z. Eleme, S. Harissopoulos, A. Kalamara, K. Karfopoulos, M. Kokkoris *et al.*, *Experimental Study of the $^{165}\text{Ho}(n,2n)$ Reaction: Cross Section Measurements for the Population of the ^{164}Ho Ground State and Isomeric State from the Threshold up to 20 MeV*, Phys. Rev. C **102**, 034610 (2020).
- [45] J. A. Frenje, *Nuclear Diagnostics for Inertial Confinement Fusion (ICF) Plasmas*, Plasma Phys. Control. Fusion **62**, 023001 (2020).
- [46] C. J. Cerjan, L. Bernstein, L. B. Hopkins, R. M. Bionta, D. L. Bleuel, J. A. Caggiano, W. S. Cassata, C. R. Brune, J. Frenje, M. Gatu-Johnson *et al.*, *Dynamic High Energy Density Plasma Environments at the National Ignition Facility for Nuclear Science Research*, J. Phys. G Nucl. Part. Phys. **45**, 033003 (2018).
- [47] J. Kawanaka, N. Miyanaga, H. Azechi, T. Kanabe, T. Jitsuno, K. Kondo, Y. Fujimoto, N. Morio, S. Matsuo, Y. Kawakami *et al.*, *3.1-KJ Chirped-Pulse Power Amplification in the LFEX Laser*, *Journal of Physics: Conference Series*, (IOP Publishing, Bristol, 2008), **112**, 032006.
- [48] A. Yogo, K. Mima, N. Iwata, S. Tosaki, A. Morace, Y. Arikawa, S. Fujioka, T. Johzaki, Y. Sentoku, H. Nishimura *et al.*, *Boosting Laser-Ion Acceleration with Multi-Picosecond Pulses*, Sci. Rep. **7**, 42451 (2017).
- [49] D. O. Golovin, S. R. Mirfayzi, S. Shokita, Y. Abe, Z. Lan, Y. Arikawa, A. Morace, T. A. Pikuz, and A. Yogo, *Calibration of Imaging Plates Sensitivity to High Energy Photons and Ions for Laser-Plasma Interaction Sources*, J. Instrum. **16**, T02005 (2021).
- [50] J. Fuchs, Y. Sentoku, E. D'Humières, T. E. Cowan, J. Cobble, P. Audebert, A. Kemp, A. Nikroo, P. Antici, E. Brambrink *et al.*, *Comparative Spectra and Efficiencies of Ions Laser-Accelerated Forward from the Front and Rear Surfaces of Thin Solid Foils*, Phys. Plasmas **14**, 053105 (2007).
- [51] M. Lugaro, A. Heger, D. Osrin, S. Goriely, K. Zuber, A. I. Karakas, B. K. Gibson, C. L. Doherty, J. C. Lattanzio, and U. Ott, *Stellar Origin of the ^{182}Hf Cosmochronometer and the Presolar History of Solar System Matter*, Science **345**, 6197 (2014).
- [52] K. Wisshak, F. Voss, F. Käppeler, L. Kazakov, F. Bečvář, M. Krtička, R. Gallino, and M. Pignatari, *Fast Neutron Capture on the Hf Isotopes: Cross Sections, Isomer Production, and Stellar Aspects*, Phys. Rev. C **73**, 045807 (2006).
- [53] Y. Abe, H. Hosoda, Y. Arikawa, T. Nagai, S. Kojima, S. Sakata, H. Inoue, Y. Iwasa, K. Iwano, K. Yamanoi *et al.*, *Characterizing a Fast-Response, Low-Afterglow Liquid Scintillator for Neutron Time-of-Flight Diagnostics in Fast Ignition Experiments*, Rev. Sci. Instrum. **85**, 11E126 (2014).
- [54] R. J. Gehrke and J. R. Davidson, *Acquisition of Quality γ -Ray Spectra with HPGe Spectrometers*, Appl. Radiat. Isot. **62**, 479 (2005).
- [55] K. Shibata, O. Iwamoto, T. Nakagawa, N. Iwamoto, A. Ichihara, S. Kunieda, S. Chiba, K. Furutaka, N. Otuka, T. Ohsawa *et al.*, *JENDL-4.0: A New Library for Nuclear Science and Engineering*, J. Nucl. Sci. Technol. **48**, 1 (2011).
- [56] T. Sato, Y. Iwamoto, S. Hashimoto, T. Ogawa, T. Furuta, S. Abe, T. Kai, P. E. Tsai, N. Matsuda, H. Iwase *et al.*, *Features of Particle and Heavy Ion Transport Code System (PHITS) Version 3.02*, J. Nucl. Sci. Technol. **55**, 684 (2018).

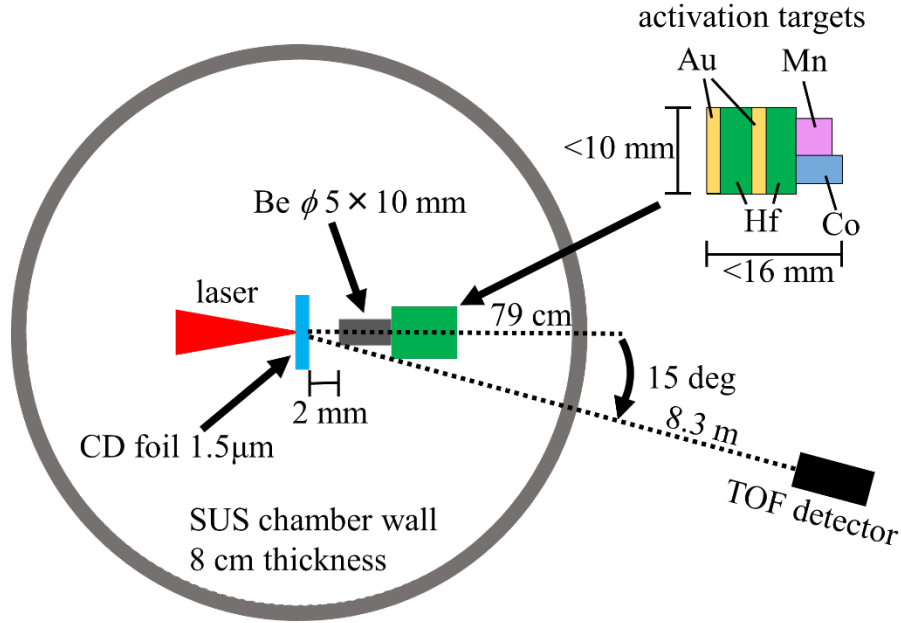


FIG. 1. Experimental layout of the fast neutron generation for the short L3658. In this experiment, the ^9Be target was used as a neutron converter. The neutrons emit almost isotropically. The neutrons were exposure on the activation targets on the laser axis, and were measured with a TOF detector located outside of the chamber.

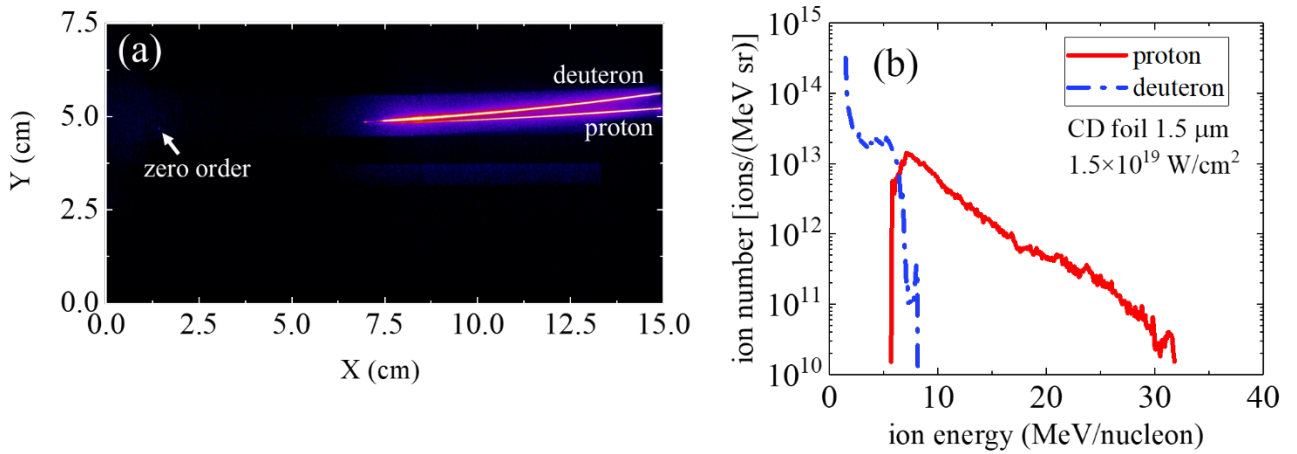


FIG. 2. **Signals of laser-accelerated protons and deuterons.** (a) Image of the IP located behind the Thomson Parabola Ion Spectrometer, which was recorded on the shot L3651. The tracks of the protons and the deuterons are clearly appeared. (b) Ion energy spectra of the shot L3651 evaluated from the tracks on the IP. The red solid and blue dashed lines present the energy spectra of the protons and the deuterons, respectively.

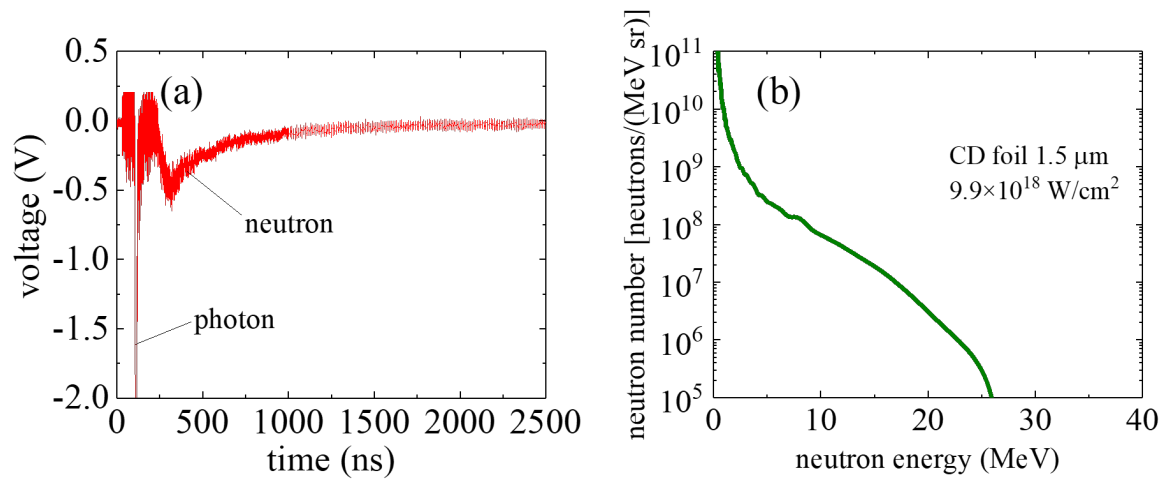


FIG. 3. **Results of neutron TOF measurements.** (a) The output from the scintillation detector located at 15 deg away from the laser axis and a distance of 8.3 m on the shot L3658. The output was recorded with an oscilloscope shot by shot. Neutron and photon signals were clearly separated. (b) Fast neutron spectrum evaluated from the output of the scintillation detector. The neutrons with energies of up to 26 MeV were measured.

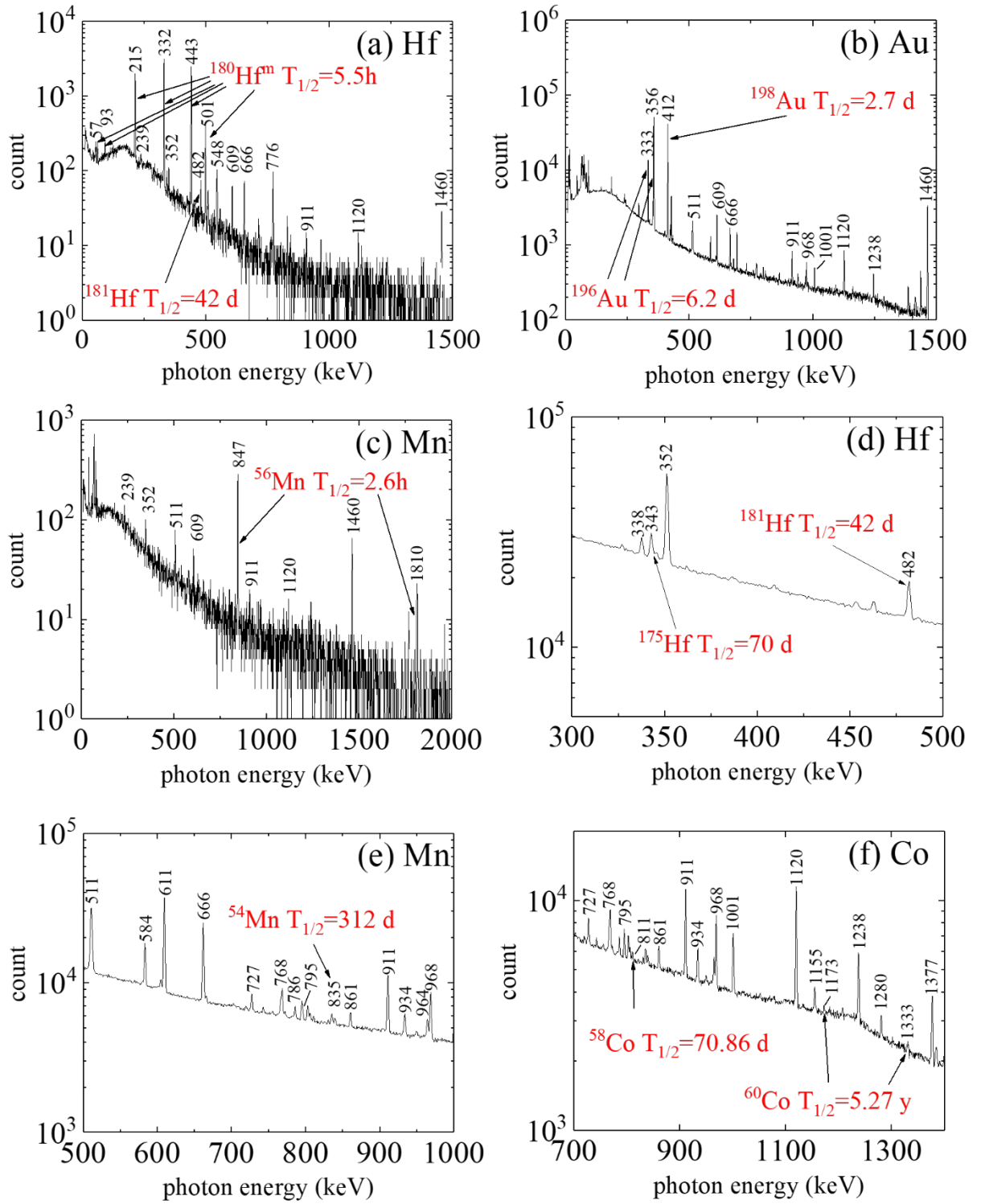


FIG. 4. γ -ray spectra for (a) $^{180}\text{Hf}^m$, (b) $^{196,198}\text{Au}$, (c) ^{56}Mn , (d) $^{175,181}\text{Hf}$, (e) ^{54}Mn , and (f) $^{58,60}\text{Co}$. These spectra were measured using the three HPGe detectors with the shields after laser shots.

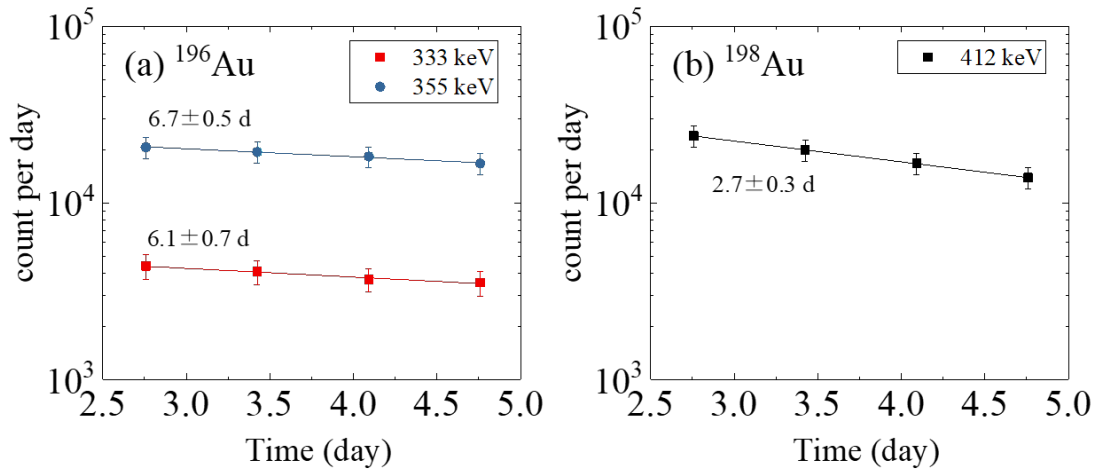


FIG. 5. Results of half-life measurements of ^{196}Au and ^{198}Au . (a) Measured decay curves of 333-keV and 355-keV γ -rays radiated from ^{196}Au that is generated by the $^{197}\text{Au}(n, 2n)^{196}\text{Au}$ reaction. (b) Measured decay curve of 412-keV γ -ray from ^{198}Au produced by $^{197}\text{Au}(n, \gamma)^{198}\text{Au}$ reaction.

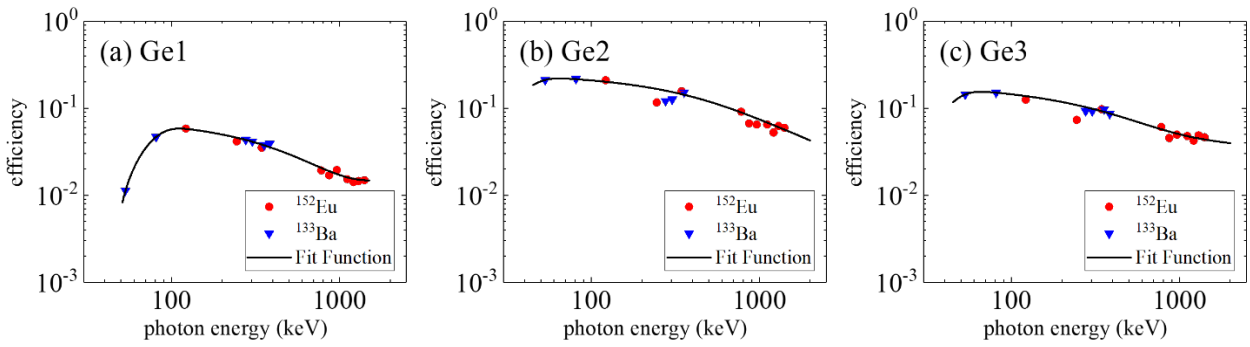


FIG. 6. Efficiency curves of the Ge detectors used to evaluate the nuclear reaction rate per nucleus. (a), (b), and (c) shows efficiency curve of Ge1, Ge2, and Ge3, respectively.

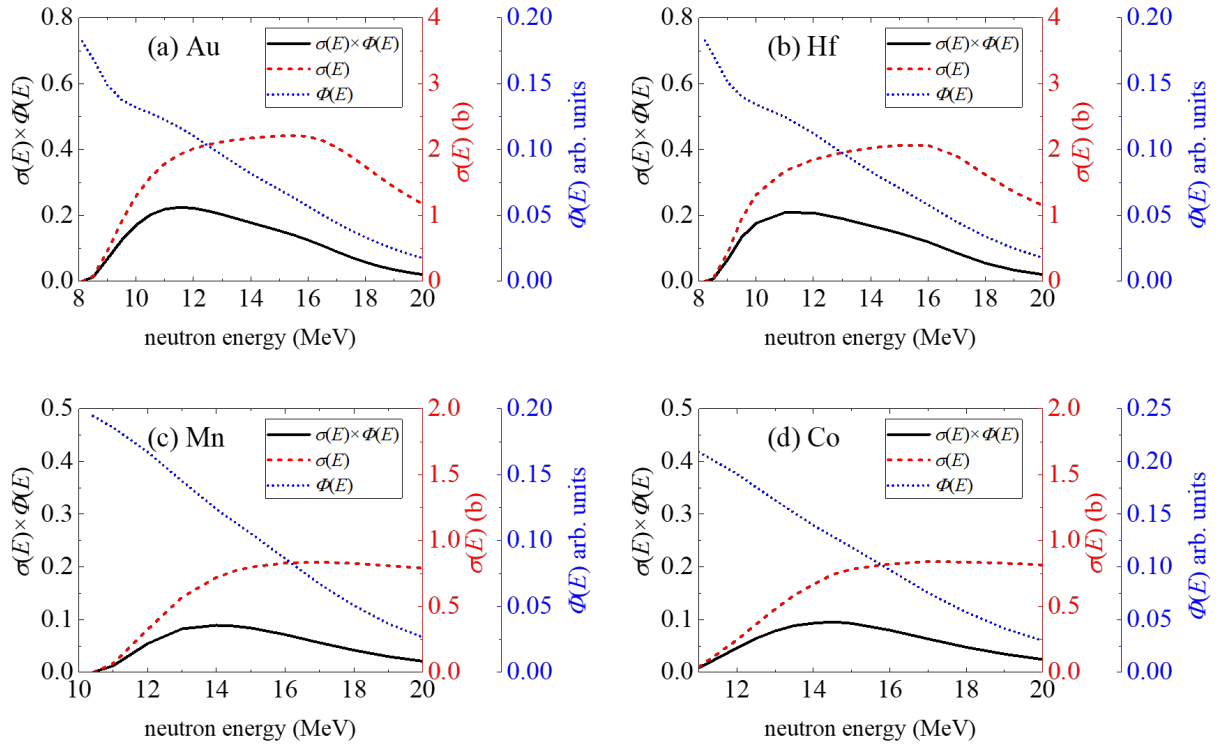


FIG. 7. The $(n, 2n)$ reaction cross sections on ^{176}Hf , ^{197}Au , ^{55}Mn , and ^{59}Co , the measured neutron energy spectra provided from the LDNS, and their product. The blue dotted lines show the normalized neutron energy spectrum. The red dashed lines show $(n, 2n)$ cross sections of each nuclides. The black solid lines show the product of the $(n, 2n)$ cross section multiplied by the normalized neutron spectrum for each nuclide.

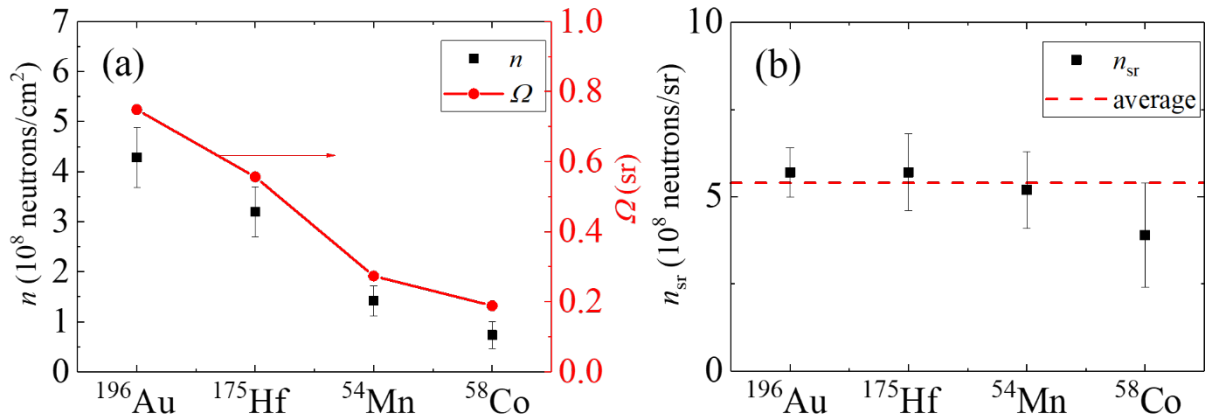


FIG. 8. Evaluated neutron fluxes from the activation method using $(n, 2n)$ reactions. (a) 8-20 MeV neutron fluence measured by the $(n, 2n)$ activation method and solid angles of the targets from neutron generation point in the Be converter and (b) the neutron yield for each target. The dashed line shows that the average yield.

TABLE I. Neutron irradiation targets and its purity, isotopic abundance of each isotope, mass, size, and shape.

Irradiation targets and purity of the element (natural abundance of the isotopes)	Target mass (mg)	Size and shape
Hf, 97% (¹⁷⁴ Hf: 0.16%, ¹⁷⁶ Hf: 5.26%, ¹⁷⁷ Hf: 18.6%, ¹⁷⁸ Hf: 27.28%, ¹⁷⁹ Hf: 13.62%, ¹⁸⁰ Hf: 35.08%)	5545.05	ϕ 9 mm \times 1mmt, 6 discs
Au, 99.95% (¹⁹⁷ Au: 100%,)	2423.72	ϕ 9 mm \times 1mmt, 2 discs
Mn, 99.999% (⁵⁵ Mn: 100%)	1034.57	About 300 mm ³ , 1 shot
Co, 99.98% (⁵⁹ Co: 100%)	312.03	About 125 mm ³ , 1 shot

TABLE II. The energy, the half-life of the parent nuclide, and the emission probability per decay of each measured γ -ray from unstable isotopes generated by the neutron-induced reactions.

Energy (keV)	Radionuclide identification	Emission probability (%)
57.6	¹⁸⁰ Hf ^m	51.0
93.3	¹⁸⁰ Hf ^m	18.2
215.3	¹⁸⁰ Hf ^m	86.4
332.3	¹⁸⁰ Hf ^m	100.0
333.0	¹⁹⁶ Au	26.3
343.4	¹⁷⁵ Hf	84.0
355.7	¹⁹⁶ Au	100.0
411.8	¹⁹⁸ Au	100
443.2	¹⁸⁰ Hf ^m	87.0
482.2	¹⁸¹ Hf	80.5
500.7	¹⁸⁰ Hf ^m	15.2
810.8	⁵⁸ Co	99.0
834.8	⁵⁴ Mn	99.9
846.8	⁵⁶ Mn	98.9
1173	⁶⁰ Co	99.9
1333	⁶⁰ Co	99.9
1810	⁵⁶ Mn	27.2

TABLE III. The energy, the half-life of the parent nuclide, and the emission probability per decay of each measured γ -ray radiated from the natural radionuclides.

Energy (keV)	Radionuclide identification	Emission probability (%)
46.5	²¹⁰ Pb	4.25

186.2	^{226}Ra	3.5
238.6	$^{212}\text{Pd}(^{232}\text{Th})$	100.0
351.9	^{214}Pb	37.6
510.8	^{208}Tl and e^-+e^+ annihilation	22.6 and 200 or more
583.2	^{208}Tl	84.5
609.3	$^{214}\text{Bi}(^{226}\text{Ra})$	46.1
661.7	^{137}Cs	85.1
665.5	$^{214}\text{Bi}(^{226}\text{Ra})$	1.29
727.3	$^{212}\text{Bi}(^{232}\text{Th})$	6.58
768.4	$^{214}\text{Bi}(^{226}\text{Ra})$	4.94
785.7	^{214}Pb	1.07
794.9	$^{228}\text{Ac}(^{232}\text{Th})$	4.25
860.6	^{208}Tl	12.4
911.2	$^{228}\text{Ac}(^{232}\text{Th})$	26.6
934	$^{214}\text{Bi}(^{226}\text{Ra})$	3.0
968	$^{228}\text{Ac}(^{232}\text{Th})$	16.2
1001	$^{234}\text{Pa}^m$	0.837
1120	$^{214}\text{Bi}(^{226}\text{Ra})$	14.8
1155	$^{214}\text{Bi}(^{226}\text{Ra})$	1.6
1238	$^{214}\text{Bi}(^{226}\text{Ra})$	5.8
1280	$^{214}\text{Bi}(^{226}\text{Ra})$	1.4
1377	$^{214}\text{Bi}(^{226}\text{Ra})$	4.0
1385	$^{214}\text{Bi}(^{226}\text{Ra})$	0.76
1402	$^{214}\text{Bi}(^{226}\text{Ra})$	1.3
1408	$^{214}\text{Bi}(^{226}\text{Ra})$	2.2
1460	^{40}K	10.7
1509	$^{214}\text{Bi}(^{226}\text{Ra})$	2.1

TABLE IV. Isotopes and isomer production reaction rate per nucleus measured by Ge detectors.

Nuclide	r (nucleus $^{-1}$)
^{175}Hf	$(5.0\pm 0.9)\times 10^{-16}$
$^{180}\text{Hf}^m$	$(6.2\pm 0.6)\times 10^{-17}$
^{181}Hf	$(1.2\pm 0.18)\times 10^{-16}$
^{196}Au	$(4.9\pm 0.5)\times 10^{-16}$
^{198}Au	$(4.9\pm 0.7)\times 10^{-16}$
^{54}Mn	$(4.9\pm 1.2)\times 10^{-17}$

^{56}Mn	$(3.4\pm 0.4)\times 10^{-18}$
^{58}Co	$(2.2\pm 0.8)\times 10^{-17}$
^{60}Co	$(2.1\pm 0.9)\times 10^{-16}$

TABLE V. 8-20 MeV neutron fluence and parameters for the present analysis.

Reaction	r (nucleus $^{-1}$)	S (b)	D	n (neutrons/cm 2)	Ω (sr)	n_{sr} (neutrons/sr)
$^{197}\text{Au}(n, 2n)^{196}\text{Au}$	$(4.9\pm 0.5)\times 10^{-16}$	1.53 ± 0.018	0.75	$(4.3\pm 0.5)\times 10^8$	0.75	$(5.7\pm 0.7)\times 10^8$
$^{176}\text{Hf}(n, 2n)^{175}\text{Hf}$	$(5.0\pm 0.9)\times 10^{-16}$	1.46 ± 0.022	0.72	$(3.2\pm 0.6)\times 10^8$	0.56	$(5.7\pm 1.1)\times 10^8$
$^{55}\text{Mn}(n, 2n)^{54}\text{Mn}$	$(4.9\pm 1.2)\times 10^{-17}$	$(5.30\pm 0.10)\times 10^{-1}$	0.67	$(1.4\pm 0.3)\times 10^8$	0.27	$(5.2\pm 1.1)\times 10^8$
$^{59}\text{Co}(n, 2n)^{58}\text{Co}$	$(2.2\pm 0.8)\times 10^{-17}$	$(5.55\pm 0.04)\times 10^{-1}$	0.54	$(7.4\pm 2.7)\times 10^7$	0.19	$(3.9\pm 1.5)\times 10^8$